Draft version April 7, 2016
Preprint typeset using LaTeX style emulateapj v. 5/2/11

arXiv:1602.06190v2 [astro-ph.HE] 6 Apr 2016

OPTICAL TRANSIENTS POWERED BY MAGNETARS: DYNAMICS, LIGHT CURVES, AND TRANSITION TO THE NEBULAR PHASE

Ling-Jun Wang[1,2,3], S. Q. Wang[2,3], Z. G. Dai[2,3], Dong Xu[1], Yan-Hui Han[1], X. F. Wu[4,5], Jian-Yan Wei[1]
[1]Key Laboratory of Space Astronomy and Technology, National Astronomical Observatories, Chinese Academy of Sciences, Beijing 100012, China; wanglj@nao.cas.cn, wjy@nao.cas.cn
[2]School of Astronomy and Space Science, Nanjing University, Nanjing, China; dzg@nju.edu.cn
[3]Key laboratory of Modern Astronomy and Astrophysics (Nanjing University), Ministry of Education, Nanjing 210093, China
[4]Purple Mountain Observatory, Chinese Academy of Sciences, Nanjing, 210008, China and
[5]Joint Center for Particle Nuclear Physics and Cosmology of Purple Mountain Observatory-Nanjing University, Chinese Academy of Sciences, Nanjing 210008, China

Draft version April 7, 2016

ABSTRACT

Millisecond magnetars can be formed via several channels: core-collapse of massive stars, accretion-induced collapse of white dwarfs (WDs), double WD mergers, double neutron star (NS) mergers, and WD-NS mergers. Because the mass of ejecta from these channels could be quite different, their light curves are also expected to be diverse. We evaluate the dynamic evolution of optical transients powered by millisecond magnetars. We find that the magnetar with short spin-down timescale converts its rotational energy mostly into the kinetic energy of the transient, while the energy of a magnetar with long spin-down timescale goes into radiation of the transient. This leads us to speculate that hypernovae could be powered by magnetars with short spin-down timescales. At late times the optical transients will gradually evolve into a nebular phase because of the photospheric recession. We treat the photosphere and nebula separately because their radiation mechanisms are different. In some cases the ejecta could be light enough that the magnetar can accelerate it to a relativistic speed. It is well known that the peak luminosity of a supernova (SN) occurs when the luminosity is equal to the instantaneous energy input rate, as shown by Arnett (1979). We show that photospheric recession and relativistic motion can modify this law. The photospheric recession always leads to a delay of the peak time $t_{\rm pk}$ relative to the time $t_\times$ at which the SN luminosity equals the instantaneous energy input rate. Relativistic motion, however, may change this result significantly.

Subject headings: radiation mechanisms: thermal — stars: neutron — supernovae: general

1. INTRODUCTION

The discovery of superluminous supernovae (SLSNe; Chomiuk et al. 2011; Quimby et al. 2011; Gal-Yam 2012) in the last decade has greatly expanded the SN family and its astrophysical significance, thanks to the unbiased wide surveys such as the Panoramic Survey Telescope and Rapid Response System (Pan-STARRS), the Palomar Transient Factory (PTF; Law et al. 2009; Rau et al. 2009), the Catalina Realtime Transient Survey (CRTS; Drake et al. 2009), and the La Silla QUEST survey (LSQ; Baltay et al. 2013).

To date the observed SLSNe can be classified into two categories, viz. type Ic SLSNe and type IIn SLSNe[1]. Type IIn SLSNe show strong signs of circumstellar interaction. Type Ic SLSNe, on the other hand, are usually assumed to be energized by newborn millisecond magnetars during the core collapse of the progenitors (Kasen & Bildsten 2010; Woosley 2010; Chatzopoulos et al. 2012, 2013; Inserra et al. 2013; McCrum et al. 2014; Nicholl et al. 2014; Papadopoulos et al. 2015; Wang et al. 2015b,c; Dai et al. 2016; Metzger et al. 2015; Mösta et al. 2015)[2].

Other channels to form millisecond magnetars include accretion-induced collapse of white dwarfs (AIC; Canal & Schatzman 1976; Ergma & Tutukov 1976; Nomoto & Kondo 1991; Usov 1992), double white dwarf (WD) mergers (Saio & Nomoto 1985; Levan et al. 2006b), double neutron star mergers (NSM; Dai & Lu 1998a,b; Dai et al. 2006; Zhang 2013; Giacomazzo & Perna 2013), and WD-NS mergers (Metzger 2012). AIC and NSM are of particular interest here because AIC ejects an outflow with mass $M_{\rm ej} = 10^{-3} - 10^{-1} M_\odot$ (Dessart et al. 2006), while NSM results in ejecta with masses $M_{\rm ej} = 10^{-4} - 10^{-2} M_\odot$ and velocity $v = 0.1 - 0.3c$ (Rezzolla et al. 2010; Hotokezaka et al. 2013; Rosswog et al. 2013). Such low masses of the ejecta can be accelerated to quasi-relativistic speed by the magnetar.

The magnetar-powered optical transients, e.g. a fraction of SLSNe that are believed to be powered by magnetars, are usually modeled based on the analytical solution developed by Arnett (1980, 1982), who assumed that the kinetic energy of the SNe is constant and the ejecta of the SNe are dense enough that the photosphere does not recede. This simple solution works pretty well in reproducing the observational data except for some cases which render excess in theoretical light curves compared with the observational data in late times (Inserra et al. 2013; Nicholl et al. 2014). To rescue the magnetar model, it is arguably suggested (Wang et al. 2015c) that the energy injected from the rotating magnetar could leak away from the ejecta based on the observation that the spin-down luminosity of the magnetar could be dominated by high

[1] A few SLSNe are classified as type IIL.
[2] It is suggested that the luminous supernovae show evidence for both ^{56}Ni and magnetars (Wang et al. 2015d).

energy gamma rays (Caraveo 2014).

The analytical model usually treats with the ejecta as a whole, even if the SN goes into a nebular phase in late times. Arnett & Fu (1989) considered the photospheric recession resulting from the ion recombination. In their model the ejecta interior of the photosphere are continuously heated by the radioactive decay of ^{56}Ni and ^{56}Co while the ejecta exterior are cool and transparent that emanates no radiation. In this paper we consider the photospheric recession and treat the ejecta within and outside of the photosphere separately so that the SN can transit from the photospheric phase into a nebular phase smoothly. Our aim at present is not to elaborate a full-fledged model of the nebular phase of the SN. But rather, as a first step, we would like to demonstrate how the nebular emission takes over the photospheric emission. In future a more elaborated model can be developed based on this model.

A significant fraction of the magnetar's rotational energy can be converted into the SN kinetic energy. As a result, the acceleration of the SN by the magnetar should be taken into consideration. In Section 2 we present our model, taking into account the dynamic evolution, photospheric recession, nebular phase takeover. In the extreme case for very light ejecta, the SN can be boosted to a quasi-relativistic speed. We present the light curves and temperature evolution in Section 3 in the relativistic case. Finally, discussions and conclusions are given in Section 4.

2. AN ANALYTICAL SN MODEL THAT TREATS PHOTOSPHERE AND NEBULA SEPARATELY

We assume a constant density and homologous expansion of the SN. An ordinary SN is heated by the ^{56}Ni and ^{56}Co decay (Colgate & McKee 1969; Colgate et al. 1980; Arnett 1980, 1982)

$$L_{\rm Ni}(t) = M_{\rm Ni}\left[(\epsilon_{\rm Ni}-\epsilon_{\rm Co})\,e^{-t/\tau_{\rm Ni}}+\epsilon_{\rm Co}e^{-t/\tau_{\rm Co}}\right], \quad (1)$$

where $M_{\rm Ni}$ is the mass of ^{56}Ni, $\epsilon_{\rm Ni} = 3.9\times 10^{10}\,{\rm erg\,g^{-1}\,s^{-1}}$, $\epsilon_{\rm Co} = 6.78\times 10^{9}\,{\rm erg\,g^{-1}\,s^{-1}}$, $\tau_{\rm Ni}$ and $\tau_{\rm Co}$ are the lifetime of ^{56}Ni and ^{56}Co, respectively. For a magnetar-powered SLSN, the energy source is the spin-down luminosity of the magnetar (Ostriker & Gunn 1971)

$$L_{\rm mag}(t) = \frac{E_{\rm sd}}{\tau_{\rm sd}\left(1+t/\tau_{\rm sd}\right)^2}, \quad (2)$$

where $\tau_{\rm sd} = 2.3\,{\rm days} R_{*,6}^{-6}B_{p,14}^{-2}P_{0,-3}^{2}$ is the spin-down timescale of the magnetar, $E_{\rm sd} = L_{\rm sd,0}\tau_{\rm sd}$, $L_{\rm sd,0} = 10^{47}\,{\rm erg\,s^{-1}}P_{0,-3}^{-4}B_{p,14}^{2}R_{*,6}^{6}$ the spin-down luminosity of the magnetar, B_p the magnetar's dipole magnetic field, P_0 its initial spin period, R_* its radius. Here the usual convention $Q = 10^{n}Q_n$ is adopted.

After taking into account the gamma-ray leakage, the radioactive decay input within the photosphere is modified as

$$L_{\rm Ni}^{\rm SN}(t) = L_{\rm Ni}(t)\left(1-e^{-\tau_{\gamma,\rm Ni}^{\rm SN}}\right), \quad (3)$$

where the optical depth of the SN within photosphere to the ^{56}Ni and ^{56}Co decay photons $\tau_{\gamma,\rm Ni}^{\rm SN}$ is given by

$$\tau_{\gamma,\rm Ni}^{\rm SN} = \frac{3\kappa_{\gamma,\rm Ni}M_{\rm ej}x_{\rm ph}}{4\pi R^2}. \quad (4)$$

Here $\kappa_{\gamma,\rm Ni}$ is the opacity to the ^{56}Ni and ^{56}Co decay photons, $R(t)$ the SN radius (including the nebula) at time t, and $x_{\rm ph} = v_{\rm ph}/v_{\rm sc}$. $v_{\rm sc}$ is the velocity scale which is approximately the photospheric velocity $v_{\rm ph}$ at the SN peak luminosity when the photosphere does not recede yet. In the homologous approximation, the (relative) Lagrangian space coordinate of a fluid element is $x = r/R(t)$.

Similarly, the spin-down luminosity taking into account the gamma-ray leakage is

$$L_{\rm mag}^{\rm SN}(t) = L_{\rm mag}(t)\left(1-e^{-\tau_{\gamma,\rm mag}^{\rm SN}}\right), \quad (5)$$

where

$$\tau_{\gamma,\rm mag}^{\rm SN} = \frac{3\kappa_{\gamma,\rm mag}M_{\rm ej}x_{\rm ph}}{4\pi R^2} \quad (6)$$

and $\kappa_{\gamma,\rm mag}$ is the opacity to the gamma-ray photons from the magnetar. Because the ^{56}Ni gamma-ray spectrum is different from that from the spinning-down magnetar, $\kappa_{\gamma,\rm mag}$ is generally not the same as $\kappa_{\gamma,\rm Ni}$. As can be appreciated, the superscript SN in this paper indicates the quantity within the SN photosphere, while the superscript atm in the below context indicates the quantity within the SN nebula.

In the approximation of a constant expansion rate and that the initial radius $R(0)$ of the SN can be ignored, the radius of the SN is given by $R = v_{\rm sc}t$. As a result the optical depth of the SN to the gamma-rays within photosphere is given by

$$\tau_{\gamma}^{\rm SN} = At^{-2}, \quad (7)$$

where

$$A = \frac{3\kappa_{\gamma}M_{\rm ej}}{4\pi v_{\rm sc}^2}. \quad (8)$$

Here κ_γ can be $\kappa_{\gamma,\rm mag}$ or $\kappa_{\gamma,\rm Ni}$, whatever suitable.

In the approximation that the photosphere does not recede, i.e. $x_{\rm ph} = 1$, the luminosity is given by (Arnett 1982)

$$L(1,t) = \frac{E_{\rm th}(0)}{\tau_0}\phi(t), \quad (9)$$

where the "1" in $L(1,t)$ means the position $x = 1$, i.e. the photosphere, and $E_{\rm th}(0)$ is the initial thermal energy of the SN and the diffusion time scale τ_0 is defined as (Arnett 1980, 1982)

$$\tau_0 = \frac{\kappa M_{\rm ej}}{\tilde{\beta}cR(0)}, \quad (10)$$

where κ is the opacity in optical band, c the speed of light, and $\tilde{\beta}\simeq 13.8$. The function ϕ, with initial value $\phi(0) = 1$, evolves according to

$$\dot{\phi} = \frac{R(t)}{R(0)}\left[\frac{L_{\rm inp}^{\rm SN}(t)}{E_{\rm th}(0)}-\frac{\phi}{\tau_0}\right] \quad (11)$$

where the energy input is the sum from ^{56}Ni and magnetar

$$L_{\rm inp}^{\rm SN}(t) = L_{\rm Ni}^{\rm SN}(t)+L_{\rm mag}^{\rm SN}(t). \quad (12)$$

If the initial thermal energy of the SN can be neglected, we arrive at the following integration expression of the

luminosity[3]

$$L(t)=\frac{2}{\tau_m}e^{-\frac{t^2}{\tau_m^2}}\int_0^t e^{\frac{t'^2}{\tau_m^2}}\frac{t'}{\tau_m}L_{\rm inp}(t')\left[1-e^{-\tau_\gamma(t')}\right]dt', \tag{13}$$

where the effective diffusion timescale τ_m is given by

$$\tau_m=\left(\frac{2\kappa M_{\rm ej}}{\tilde{\beta}cv_{\rm sc}}\right)^{1/2}. \tag{14}$$

Generally the photosphere will steadily recede, in this case the photospheric emission is given by (Arnett & Fu 1989)

$$L_{\rm ph}\left(x_{\rm ph},t\right)=\frac{E_{\rm th}\left(0\right)}{\tau_0}x_{\rm ph}\phi, \tag{15}$$

where $\phi\left(t\right)$ evolves as (Arnett & Fu 1989)[4]

$$\dot{\phi}=\frac{1}{x_{\rm ph}^3}\frac{R\left(t\right)}{R\left(0\right)}\left[\frac{L_{\rm inp}^{\rm SN}\left(t\right)}{E_{\rm th}\left(0\right)}-\frac{x_{\rm ph}}{\tau_0}\phi-3x_{\rm ph}^2\frac{R\left(0\right)}{R\left(t\right)}\dot{x}_{\rm ph}\phi\right], \tag{16}$$

where we have substituted x_i in Equation (A41) of Arnett & Fu (1989) for $x_{\rm ph}$. The Lagrangian coordinate of the photosphere $x_{\rm ph}$ is given by

$$x_{\rm ph}=1-\frac{2}{3}\frac{\lambda}{R\left(t\right)}, \tag{17}$$

where $\lambda=\left(\rho\kappa\right)^{-1}$ is the mean free path of the SN photons and ρ the SN material density. The effective temperature of the photosphere is

$$T_{\rm ph}^4\left(t\right)=\frac{E_{\rm th}\left(0\right)}{4\pi R^2\sigma\tau_0}\frac{\phi}{x_{\rm ph}}. \tag{18}$$

Up to now we have not specified the evolution of the scale velocity $v_{\rm sc}$. Under the assumption of homologous expansion of the SN, the kinetic energy of the SN is given by (Arnett 1982)

$$E_{\rm SN}=\frac{3}{10}M_{\rm ej}v_{\rm sc}^2, \tag{19}$$

whereby the scale velocity can be determined as

$$v_{\rm sc}=\left[\left(\frac{5}{3}\right)\frac{2\left(E_{\rm SN,0}+E_{K,\rm inp}\right)}{M_{\rm ej}}\right]^{1/2} \tag{20}$$

Here $E_{\rm SN,0}$ is the initial kinetic energy of the SN and the kinetic energy input $E_{K,\rm inp}$ is determined by

$$\frac{dE_{K,\rm inp}}{dt}=L_K-L_{\rm ph}-L_{\rm atm}. \tag{21}$$

The energy input from the magnetar, L_K, is given by

$$L_K=L_{\rm mag}\left(t\right)\left(1-e^{-\tau_{\gamma,\rm mag}}\right), \tag{22}$$

[3] This is the equation used by Dai et al. (2016), which is different from the widely used equation in the literature (e.g., Chatzopoulos et al. 2012), which puts the gamma-ray leakage factor outside of the integration.

[4] Equation (A41) in Arnett & Fu (1989) is in error. The correct one should read

$$\frac{d\phi}{dz}=\frac{\sigma}{x_i^3}\left[p_1\zeta\left(t\right)-p_2x_i\phi-3x_i^2\frac{\phi}{\sigma}\frac{dx_i}{dz}\right],$$

where p_1, p_2 are defined by Equations (A20) and (A21) in Arnett & Fu (1989), respectively.

where the optical depth of the SN (including the nebula) to the gamma-ray from the magnetar is given by

$$\tau_{\gamma,\rm mag}=\frac{3\kappa_{\gamma,\rm mag}M_{\rm ej}}{4\pi R^2}. \tag{23}$$

The nebular luminosity, $L_{\rm atm}$, in Equation (21) will be determined as follows.

For the nebular component of the SN, i.e. the part outside of the photosphere of the SN, we assume a homogeneous density and temperature distribution. In this approximation, the nebular luminosity is

$$L_{\rm atm}=\frac{E_{\rm atm}c}{R\left(1-x_{\rm ph}\right)}, \tag{24}$$

where the internal energy of the nebula evolves according to

$$\frac{dE_{\rm atm}}{dt}+P\frac{dV_{\rm atm}}{dt}=L_{\rm inp}^{\rm atm}-L_{\rm atm}-4\pi R^3x_{\rm ph}^2aT_{\rm ph}^4\frac{dx_{\rm ph}}{dt}. \tag{25}$$

Obviously, the volume of the nebula is

$$V_{\rm atm}=\frac{4}{3}\pi R^3\left(1-x_{\rm ph}^3\right). \tag{26}$$

In Equation (25) the first term on the right hand side is the energy input from magnetar and ^{56}Ni

$$L_{\rm inp}^{\rm atm}=L_{\rm Ni}^{\rm atm}\left(t\right)+L_{\rm mag}^{\rm atm}\left(t\right), \tag{27}$$

which is the sum of the following two terms

$$L_{\rm Ni}^{\rm atm}\left(t\right)=L_{\rm Ni}\left(t\right)\left(e^{-\tau_{\gamma,\rm Ni}^{\rm SN}}-e^{-\tau_{\gamma,\rm Ni}}\right), \tag{28}$$

$$L_{\rm mag}^{\rm atm}\left(t\right)=L_{\rm mag}\left(t\right)\left(e^{-\tau_{\gamma,\rm mag}^{\rm SN}}-e^{-\tau_{\gamma,\rm mag}}\right). \tag{29}$$

Finally the nebular temperature is

$$T_{\rm atm}=\left(\frac{E_{\rm atm}}{aV_{\rm atm}}\right)^{1/4}. \tag{30}$$

Having elaborated our analytical model, we would like to evaluate the model against observational data. First of all, because the magnetar can deposit a significant fraction of its rotational energy as the kinetic energy of the SN, the expansion velocity of the SN is actually not a constant, as is usually assumed in the previous analytical models. However, since the magnetar dissipates its rotational energy in a timescale $\tau_{\rm sd}=2.3\,{\rm days}R_6^{-6}B_{p,14}^{-2}P_{0,-3}^2$ the boost of the SN kinetic energy by magnetar cannot be observed given the fact that the typical SNe are detected several days after their explosion when the magnetars have already exhausted their rotational energy.

The SN light curve rises to its maximum roughly in the effective diffusion timescale τ_m. To clearly observe the acceleration of the SN by magnetar, the condition $\tau_{\rm sd}\gtrsim\tau_m$ should be guaranteed, which leads to the following upper bound on the magnetar dipole field strength

$$B_{p,14}\lesssim 0.25R_6^{-3}P_{0,-3}\left(\frac{v_{\rm sc,9}}{\kappa_{-1}M_{\rm ej,1}}\right)^{1/4}, \tag{31}$$

where the typical parameters $v_{\rm sc}=10^9\,{\rm cm\,s^{-1}}$, $\kappa=0.1\,{\rm cm^2\,g^{-1}}$, $M_{\rm ej}=10M_\odot$ are adopted. In the above expression we assume that the initial explosion energy of

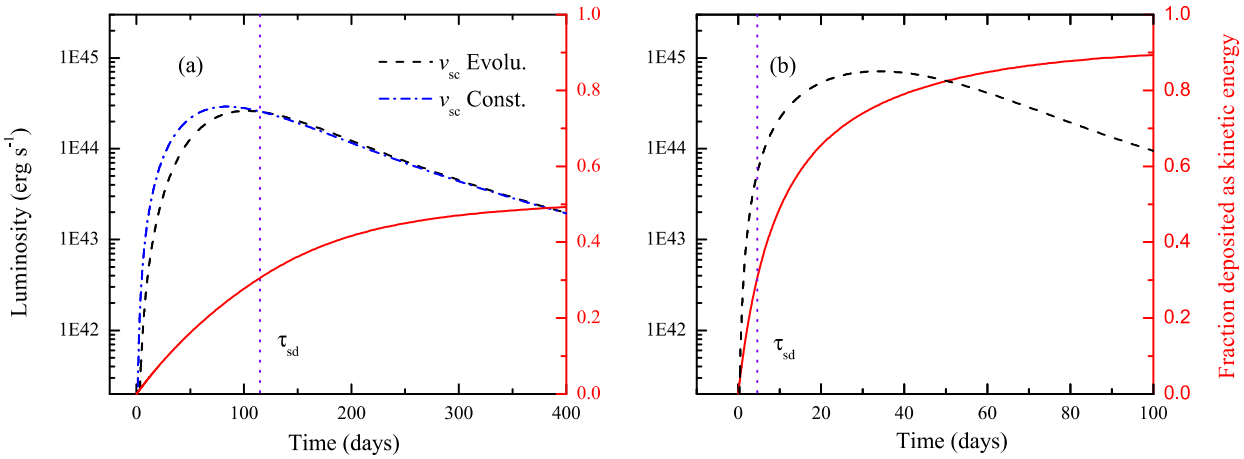

FIG. 1.— SN light curves (dashed lines) for the parameters $M_{\rm ej}=10M_\odot$, $B_p=2\times10^{13}$ G, $P_0=1.4$ ms (panel a, i.e. the case $\tau_{\rm sd}\gtrsim\tau_m$) and $M_{\rm ej}=10M_\odot$, $B_p=10^{14}$ G, $P_0=1.4$ ms (panel b, i.e. the case $\tau_{\rm sd}\ll\tau_m$). The solid lines (right vertical axis) show the accumulative fraction of the rotational energy of the magnetar converted to the kinetic energy of the SN. Vertical dotted lines mark the time $\tau_{\rm sd}$. Panel (a) also compares the SN light curves calculated by taking into account the acceleration of SN by the magnetar (dashed line) and that expected in a constant-velocity model (dot-dashed line). Note that for rendering clarity, the abscissa time internals are different between these two panels.

the SN, $E_{\rm SN}$, is larger than the energy deposited as kinetic energy by the magnetar. This is however not always true. If we assume that a fraction η_K of the rotational energy of the magnetar can be deposited as the kinetic energy of the SN, the magnetar along can accelerate the SN to a velocity

$$v_{\rm sc}=1.8\times10^9\,{\rm cm\,s^{-1}}\eta_K^{1/2}I_{45}^{1/2}M_{\rm ej,1}^{-1/2}P_{0,-3}^{-1}, \quad (32)$$

where I is the moment of inertia of the magnetar. Obviously, for less massive ejecta, the SN can be accelerated to high speed by a rapidly rotating magnetar. Provided that the kinetic energy of the SN is dominantly attributed to the magnetar, to fulfil the condition $\tau_{\rm sd}\gtrsim\tau_m$, we have

$$B_{p,14}\lesssim0.26R_6^{-3}P_{0,-3}^{3/4}\kappa_{-1}^{-1/4}M_{\rm ej,1}^{-3/8}. \quad (33)$$

We find that Equations (31) and (33) give similar upper bounds on the dipole magnetic field.

In Figure 1(a) we show the effect of the kinetic energy injection by the magnetar, along with the accumulative fraction of the total rotational energy of the magnetar deposited as the kinetic energy of the SN. In Figure 1(a) the following values are adopted $B_p=2\times10^{13}$ G, $M_{\rm ej}=10M_\odot$, $P_0=1.4$ ms. In appreciating the kinetic injection effect, we set the asymptotic velocity in our model to equal to the constant velocity in the usual model. It is clear from Figure 1(a) that the kinetic injection affects the rising part of the light curve, with a luminosity dimmer than the constant velocity model. Figure 1(a) also shows that at the maximum $\eta_K\sim30\%$ of the rotational energy of the magnetar is deposited as the kinetic energy of the SN, in rough agreement with that determined by Woosley (2010). But ultimately this fraction can be as high as $\eta_K\sim50\%$. In Figure 1(a) the parameters are adopted so that the condition $\tau_{\rm sd}>\tau_m$ is fulfilled. In the opposite extreme, i.e. $\tau_{\rm sd}\ll\tau_m$, however, as can be seen from Figure 1(b), as high as $\sim100\%$ of the rotational energy of the magnetar is converted into the kinetic energy of the SN. In conclusion, we expect that in a magnetar-powered SN, $\sim50\%-\sim100\%$ of the rotational energy of the magnetar can be converted into the kinetic energy of the SN.

In this model because $v_{\rm sc}$ is no longer a constant, the effective diffusion time τ_m is not well defined. However, since the variation of $v_{\rm sc}$ is slow, we can still think of τ_m as the rising time of the light curve. Please note that the rising times of the light curves in the two panels of Figure 1 are different even other parameters are the same except the dipole magnetic field B_p. This is because the magnetar with a stronger magnetic field can accelerate the ejecta to higher speed, reducing the effective diffusion time τ_m. In short, a magnetar with a short spin-down time deposits its rotational energy mainly as the kinetic energy of the SN, while the one with a long spin-down time deposits its rotational energy mainly as the thermal radiation of the SN. We therefore conclude that for an SN to become an SLSN, the magnetar must be fast rotating with a relatively weak dipole magnetic field.

In the following calculations of this Section, we take the magnetar parameters $B_{p,14}=2$, $P_{0,-3}=1.4$, which is equivalent to $L_{\rm sd,0}=10^{47}\,{\rm erg\,s^{-1}}$ and $\tau_{\rm sd}=10^5$ s. Other parameters are $M_{\rm ej}=10M_\odot$, $\kappa=0.1\,{\rm cm^2\,g^{-1}}$, $\kappa_{\gamma,\rm mag}=0.02\,{\rm cm^2\,g^{-1}}$, $M_{\rm Ni}=0$. We set the initial explosion energy of the SN to be $E_{\rm SN}=0$.

Figure 2 shows our model light curves. A particular demonstration of the model in reproducing the observational data is exemplified in the inset. We see that at early times the photospheric emission completely dominates, whereas at late times the photospheric emission and nebular emission conspire to follow the input power of the magnetar. In this calculation the energy leakage of the magnetar is taken into account. When $R_{\rm ph}=0$, $L_{\rm atm}=L_{\rm inp}^{\rm mag}$.

We show the photospheric velocity and effective temperature in Figures 3 and 4, respectively. The effective temperature is a weighted average of the photospheric emission and nebular emission, given by

$$T_{\rm eff}=\left(\frac{L_{\rm ph}T_{\rm ph}^4+L_{\rm atm}T_{\rm atm}^4}{L_{\rm ph}+L_{\rm atm}}\right)^{1/4}. \quad (34)$$

The above averaging scheme is motivated to pick out the

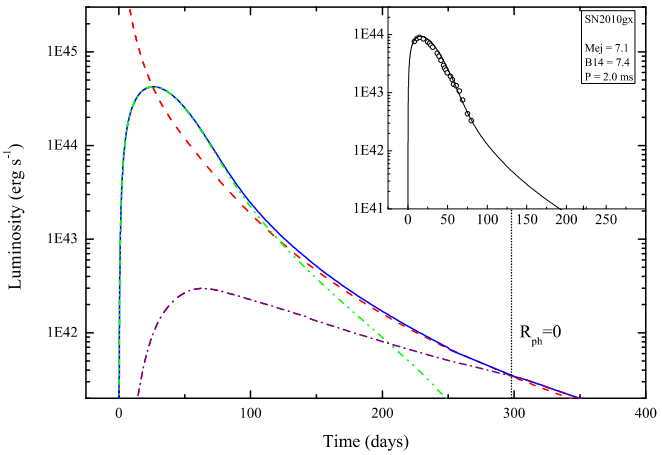

FIG. 2.— The light curves calculated according to our model with parameters $M_{\rm ej} = 10 M_\odot$, $B_p = 2 \times 10^{14}$ G, $P_0 = 1.4$ ms. In this figure we shows the bolometric luminosity (solid line), luminosity due to the photospheric emission (dot-dot-dashed line), luminosity due to the nebula (dot-dashed line), and the magnetar luminosity (dashed line). Here the energy leakage of the magnetar is taken into account. The vertical dotted line marks the time when the photosphere of the SN disappears. The inset is the fit of our model to the observational data of SN2010gx, with the fit parameters the same as that used by Inserra et al. (2013).

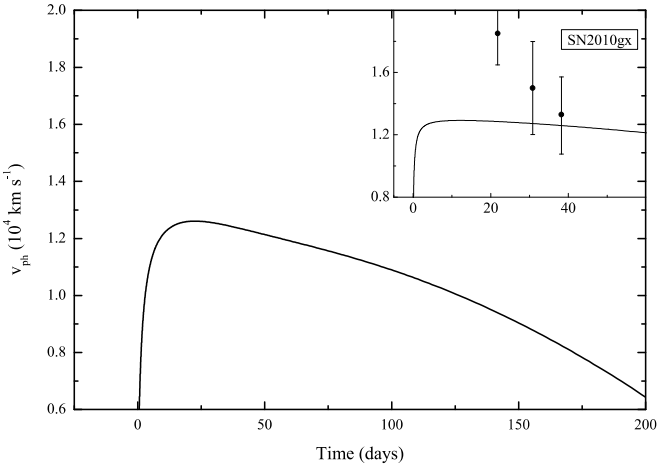

FIG. 3.— Photospheric velocity for the model parameters the same as Figure 2. The inset is the velocity evolution of SN2010gx.

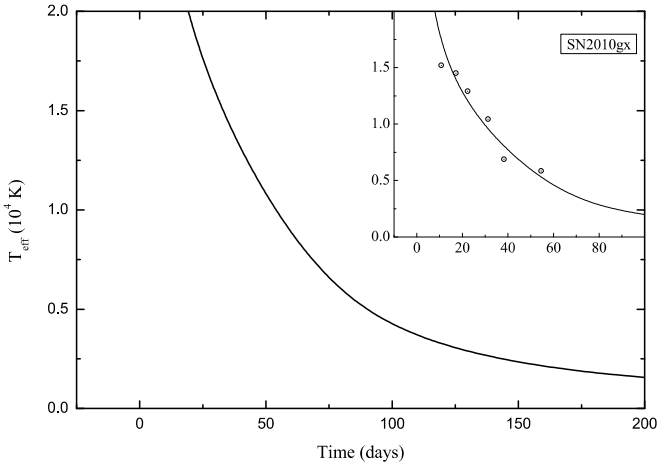

FIG. 4.— Effective temperature for the model parameters the same as Figure 2. The inset is the temperature evolution of SN2010gx.

temperature of the dominant emission component and at the same time make a smooth transition even if one of the components goes to zero.

3. RELATIVISTIC MOTION

In this section we assume that the ejecta are light enough, i.e. $M_{\rm ej} = 10^{-4} - 10^{-2} M_\odot$, so that the magnetar can accelerate it to quasi-relativistic speed. Assuming the formation of a rapidly rotating magnetar following the double neutron star merger, Yu et al. (2013) studied the merger remnant emission, dubbed merger-nova, powered by a magnetar. However, owing to some simplified assumptions underlining the calculations by Yu et al. (2013), a revisit of this problem is necessary.

The merger-nova emission, in the comoving frame, can be obtained by the method outlined in the above Section. To determine the photospheric radius of the merger-nova, we need a knowledge of the opacity. Yu et al. (2013) adopted the 'canonical' value $\kappa = 0.2\,{\rm cm^2\,g^{-1}}$, whereas we will take the newly determined value $\kappa = 10\,{\rm cm^2\,g^{-1}}$ (Barnes & Kasen 2013; Kasen et al. 2013; Tanaka & Hotokezaka 2013; Grossman et al. 2014).

Yu et al. (2013) also takes into account the deceleration of the remnant by the swept-up ambient media. We assume an ambient hydrogen number density $n = 0.1\,{\rm cm^{-3}}$, as determined in the literature (Berger et al. 2005; Soderberg et al. 2006; Berger 2007; Wang & Dai 2013). As a result, the ejecta dynamics is determined by (Yu et al. 2013)

$$\frac{d\Gamma}{dt} = \frac{\xi L_{\rm sd} + L_{\rm ra} - L_e - \Gamma \mathcal{D}\left(dE'_{\rm int}/dt'\right) - \left(\Gamma^2 - 1\right) c^2 \left(dM_{\rm sw}/dt\right)}{M_{\rm ej} c^2 + E'_{\rm int} + 2\Gamma M_{\rm sw} c^2}, \tag{35}$$

based on the generic dynamic model of GRBs (Huang et al. 1999). Here the quantities in the comoving frame are denoted by a prime. In the above equation $E'_{\rm int}$ is the internal energy of the ejecta in the comoving frame, Γ the Lorentz factor of the ejecta, $M_{\rm sw}$ the ambient mass swept up by the expanding merger-nova, L_e the bolometric luminosity of the merger-nova, t the time measured in the observer frame. The fraction of the Poynting flux caught by the ejecta is set as $\xi = 0.8$. The magnetar emission leakage is taken into account by setting $\kappa_{\gamma,{\rm mag}} = 0.02\,{\rm cm^2\,g^{-1}}$, the same as used in the above Section. The radius $R\left(t'\right)$ in Equation (16) can be obtained by a combination of Equation (35) and

$$\frac{dR}{dt} = \frac{\beta c}{1-\beta}, \tag{36}$$

where $\beta = v/c$ is the dimensionless velocity of the ejecta front.

In the comoving frame, $L'_{\rm mag} = L_{\rm mag}/\mathcal{D}^2$, where $\mathcal{D}$ is the Doppler factor. In the following calculations the mass and initial velocity of the ejecta are taken to be $M_{\rm ej} = 10^{-4}$, $10^{-2} M_\odot$ and $v = 0.2c$, in accordance with the numerical simulations (Rezzolla et al. 2010; Hotokezaka et al. 2013; Rosswog et al. 2013).

In the comoving frame, the radioactive heating rate, $L'_{\rm ra}$, of the r-process material can be well approximated according to (Korobkin et al. 2012)

$$\dot{\epsilon}\left(t'\right) = \epsilon_0 \left(\frac{1}{2} - \frac{1}{\pi} \arctan \frac{t' - t_0}{\sigma}\right)^{1.3} \left(\frac{\epsilon_{\rm th}}{0.5}\right) \tag{37}$$

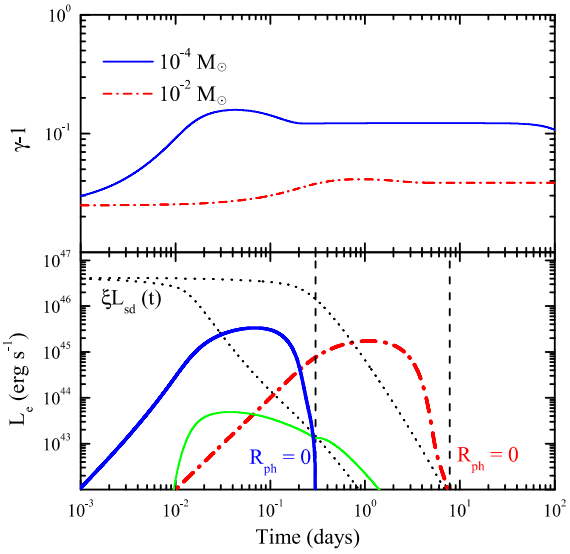

FIG. 5.— The upper panel shows the evolution of Lorentz factor. The lower panel shows the emission of photosphere (thick lines) and nebula (thin lines). The nebular emission for the $M_{\rm ej} = 10^{-2} M_\odot$ case is too low to be shown here. The dotted line is the spin down luminosity caught up by the ejecta with energy leakage considered. The vertical dashed lines mark the times when the photospheric radii vanish. The model parameters are $B_{p,14} = 2$, $P_{0,-3} = 1.4$, $\kappa = 10\,{\rm cm^2\,g^{-1}}$, $\kappa_{\gamma,{\rm mag}} = 0.02\,{\rm cm^2\,g^{-1}}$.

where $\epsilon_{\rm th}$ is the heating efficiency, and $\epsilon_0 = 2 \times 10^{18}\,{\rm erg\,g^{-1}\,s^{-1}}$, $t_0 = 1.3\,{\rm s}$, and $\sigma = 0.11\,{\rm s}$, t' the time measured in comoving frame. The heating efficiency in Equation (37) is set as $\epsilon_{\rm th} = 0.6$ to account for the energy carried away by neutrinos and the energy leak caused by gamma-ray diffusion (Metzger et al. 2010a; Roberts et al. 2011). For the typical values of the ejecta mass, the radioactive heating rate is negligible compared with the spin-down luminosity of the magnetar.

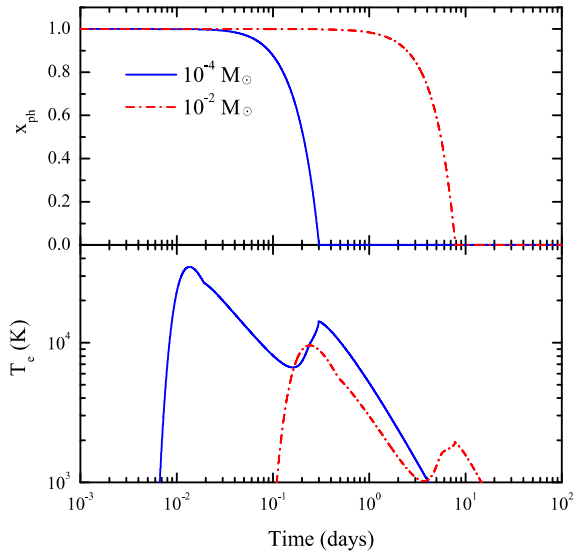

FIG. 6.— The evolution of $x_{\rm ph}$ (upper panel) and effective temperature in observer's frame (lower panel). The model parameters are the same as Figure 5.

The photospheric luminosity and flux density in the observer frame is given by $L_{\rm ph} = L'_{\rm ph}\mathcal{D}^2$ and

$$F_\nu = \frac{2\pi \mathcal{D}^2 R^2 x_{\rm ph}^2}{D_L^2 h^3 c^2 \nu} \frac{(h\nu/\mathcal{D})^4}{\exp\left(h\nu/\mathcal{D}kT'_e\right) - 1}, \qquad (38)$$

respectively. Here D_L is the distance of the merger-nova.

In Figure 5 we show the Lorentz factor and bolometric luminosities. We find that when considering the gamma-ray leakage, the ejecta can only be accelerated to sub-relativistic speed. The Lorentz factor experiences an increase and then a decline before the time when $R_{\rm ph} = 0$. This is because the merger-nova luminosity varies from a value below to a value above the magnetar input luminosity. The deceleration of the ejecta at time $t \simeq 100$ days is due to the impact of the ambient medium. In the calculations in this Section, the model parameters are $B_{p,14} = 2$, $P_{0,-3} = 1.4$, $\kappa = 10\,{\rm cm^2\,g^{-1}}$, $\kappa_{\gamma,{\rm mag}} = 0.02\,{\rm cm^2\,g^{-1}}$.

Figure 6 depicts evolution of the photospheric radius $x_{\rm ph}$ and the effective temperature T_e, weighted average expressed in (34), in the observer frame. Because the ejecta are barely relativistic, the effective temperature in the comoving frame would be very close to the observed temperature. It is found that the temperature does not monotonically decline after the first rapid rise. The second rise occurs just before the photosphere disappears. This bebaviour of the temperature evolution can be understood by comparing Figures 2 and 5. Figure 2 shows that long before $R_{\rm ph} = 0$, the nebular emission dominates over the photospheric emission, which is in sharp contrast to the situation in Figure 5. In the quasi-relativistic case, the photospheric emission dominates over the nebular emission before $R_{\rm ph} = 0$, and therefore the observed temperature reflects the photospheric emission. In this case the photosphere recedes so rapidly that the inner hot part is exposed to the observer.

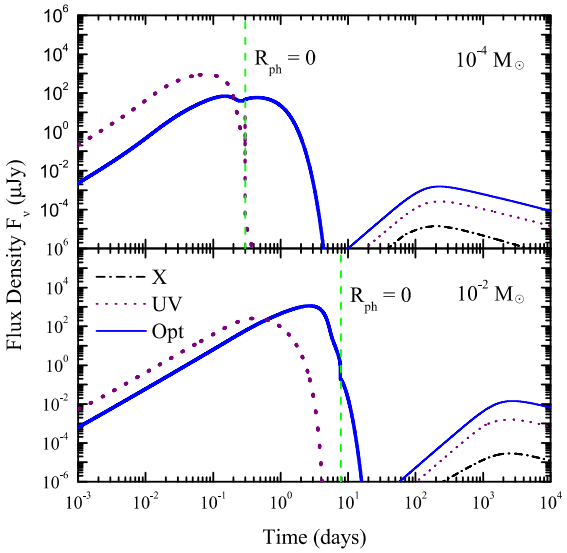

FIG. 7.— Transient emission (thick lines) and forward shock emission (thin lines) in X-ray (1 keV), UV (30 eV), and optical (606 nm) bands. The flux densities are calculated by assuming a luminosity distance $D_L = 10^{27}$ cm. Vertical dashed lines mark the times when the photospheric radii vanish. The model parameters are the same as Figure 5.

In Figure 7 we show the observed flux densities of the merger-nova emission (before $\sim$ 10 days) and for-

ward shock emission (after ~ 10 days) at optical, UV, and X-ray bands. The merger-nova emission before the time when $R_{\rm ph}=0$ comes dominantly from photosphere, thereafter the emission comes from the nebula. It is clear from this figure that the X-ray emission from merger-nova is negligible.

4. DISCUSSIONS AND CONCLUSIONS

In this paper, we develop a model for the magnetar-powered optical transients to treat the photospheric and nebular emission separately based on Arnett & Fu (1989). We also consider the quasi-relativistic merger-nova. We evaluate the acceleration of the SLSNe by the magnetar and find that this effect can be observed most clearly in the case of $\tau_{\rm sd}>\tau_m$, where $\sim 50\%$ of the magnetar rotational energy is converted to the kinetic energy of the SLSNe. In the other extreme case, i.e. $\tau_{\rm sd}\ll\tau_m$, up to 100% of the magnetar energy can be deposited as the SN kinetic energy.

It is found that the SLSNe transit from photospheric to nebular phase smoothly. When $R_{\rm ph}=0$ the nebular luminosity is equal to the instantaneous energy input rate of the magnetar. This is true for both sub-relativistic SLSNe (Figure 2) and quasi-relativistic merger-novae (Figure 5). Nevertheless we note that in this model we do not account for changes in ionization balance and hence in opacity, which could in principle affect the nebular transition.

A comparison of Figures 4 and 6 indicates that the temperature evolution could be slightly complicated if the optical transient acquires a quasi-relativistic speed. In this case, the photosphere recedes rapidly that the effective temperature could rise before the photosphere disappears.

From Equations (15) and (16) we see that for a sub-relativistic SLSN, at the maximum of the light curve, the SN luminosity equals the instantaneous energy input rate (Arnett 1979, 1982), under the assumption $x_{\rm ph}=1$ at the peak luminosity. It is clear here, because of the photospheric recession, that this law is only a good approximation. Assuming that the photospheric luminosity dominates over the nebular luminosity at the peak time $t_{\rm pk}$, Equations (15) and (16) give

$$\frac{dL_{\rm ph}}{dt}=\frac{E_{\rm th}\left(0\right)}{\tau_0 x_{\rm ph}^2}\frac{R\left(t\right)}{R\left(0\right)}\left[\frac{L_{\rm inp}^{\rm SN}\left(t\right)}{E_{\rm th}\left(0\right)}-\frac{x_{\rm ph}}{\tau_0}\phi-2x_{\rm ph}^2\frac{R\left(0\right)}{R\left(t\right)}\dot{x}_{\rm ph}\phi\right]. \tag{39}$$

Because $\dot{x}_{\rm ph}<0$, at the peak time $t_{\rm pk}$, i.e. $dL_{\rm ph}/dt=0$, the above equation gives

$$L_{\rm inp}^{\rm SN}\left(t_{\rm pk}\right)<L_{\rm ph}\left(t_{\rm pk}\right). \tag{40}$$

By assumption, $L_{\rm inp}^{\rm atm}\left(t_{\rm pk}\right)\ll L_{\rm inp}^{\rm SN}\left(t_{\rm pk}\right)$, $L_{\rm atm}\left(t_{\rm pk}\right)\ll L_{\rm ph}\left(t_{\rm pk}\right)$, in general, we have

$$t_\times<t_{\rm pk}, \tag{41}$$

where $t_\times$ is the time when the SN luminosity equals the instantaneous energy input rate.

This modification to the law $t_\times=t_{\rm pk}$ can be understood as follows. Although the photospheric recession reduces the emitting surface, it increases the surface temperature as well. These two effects result in a progressive enhancement of the photospheric luminosity, i.e. the delay of $t_{\rm pk}$ relative to $t_\times$.

If the optical transient gains a relativistic speed, Doppler transformation between the comoving frame and the observer frame may affect the above law. In the comoving frame, by definition, one have

$$L'_{\rm ph}\left(t'_\times\right)=L'_{\rm inp}\left(t'_\times\right). \tag{42}$$

In the observer frame, one have

$$L_{\rm ph}\left(t'_\times\right)=L'_{\rm ph}\left(t'_\times\right)\mathcal{D}_\times^2, \tag{43}$$

$$L_{\rm ph}\left(t'_{\rm pk}\right)=L'_{\rm ph}\left(t'_{\rm pk}\right)\mathcal{D}_{\rm pk}^2. \tag{44}$$

Because we always have $\mathcal{D}_\times>\mathcal{D}_{\rm pk}$, by demanding $t_\times=t_{\rm pk}$, i.e. $L_{\rm ph}\left(t_\times\right)=L_{\rm ph}\left(t_{\rm pk}\right)$, the condition

$$\frac{L'_{\rm ph}\left(t'_\times\right)}{L'_{\rm ph}\left(t'_{\rm pk}\right)}=\frac{\mathcal{D}_{\rm pk}^2}{\mathcal{D}_\times^2}<1 \tag{45}$$

could be fulfilled as long as the dynamic evolution of the optical transient is appropriate. The above inference indicates that it is even possible that $t_\times>t_{\rm pk}$ under relativistic motion. Figure 5 shows that the light curve of the merger-nova considered here is in the normal case, i.e. $t_\times<t_{\rm pk}$, where to be seen clearly, we depicts the horizontal axis in logarithmic scale. This is because the Doppler factor is nearly unity during the evolution of the merger-nova.

For completeness, we mention that nonhomologous expansion, e.g. shock breakout, can also modify the approximate law $t_\times=t_{\rm pk}$. Nonhomologous expansion adds the following effective source term (Arnett 1980)

$$S=-\frac{4}{3}\left(-\frac{1}{\eta}\frac{d\eta}{dx}\right)\left(\frac{v-x\dot{R}}{R}\right)T^4 \tag{46}$$

to the energy conservation equation

$$4T^4\left(\frac{\dot{T}}{T}+\frac{\dot{R}}{R}\right)=\tilde{\epsilon}+\frac{1}{r^2}\frac{\partial}{\partial r}\left(\frac{c}{3\kappa\rho}r^2\frac{\partial T^4}{\partial r}\right)+S. \tag{47}$$

Here the dimensionless function $\eta\left(x\right)$ defines the shape of the density distribution within the SN ejecta. In Equation (47) the first term on the left-hand side stands for the thermal energy, while the second term on the same side comes from the volume expansion. The first term on the right-hand side stands for the heating rate, the second term is the SN luminosity. We leave the discussion about the link between the nonhomologous heating term and the SN luminosity to the Appendix.

The term (46) has a cooling effect near the ejecta surface and a heating effect in the inner region (Arnett 1980). When the photosphere recedes inwards, the cooling effect near the surface disappears but the heating effect in the inner region remains, resulting in an enhanced luminosity relative to the homologous expansion. Shock breakout usually manifests itself as a luminosity spike, while the disappearance of the cooling effect of the surface acts as a bump in the light curve.

As an analytical model, it can be benefited from a comparison with the numerical simulations. Figure 8 is a comparison between this analytical model and the one-dimensional hydrodynamical simulations of Kasen & Bildsten (2010). It can be seen that the luminosity calculated by the analytical model is higher than

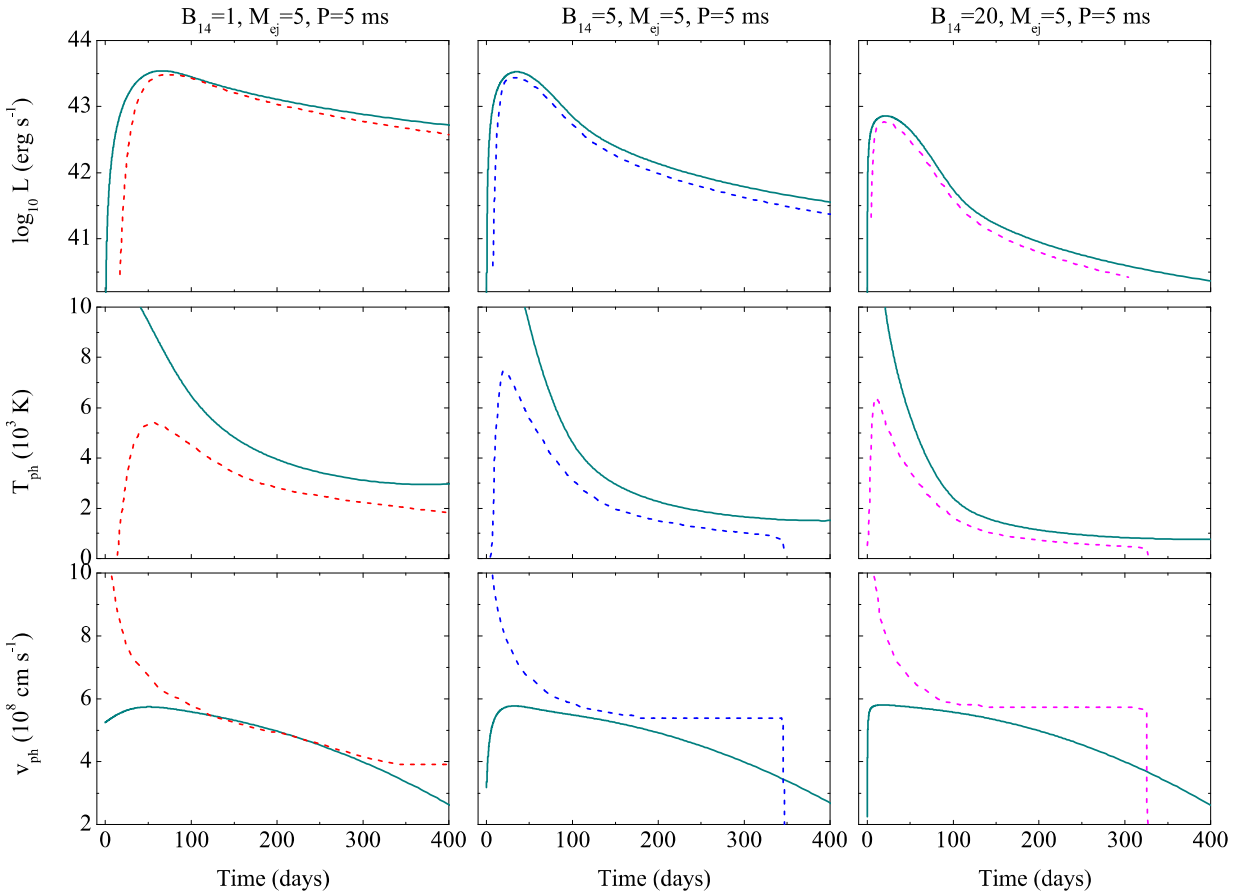

FIG. 8.— Comparison of light curves, photospheric temperatures, and photospheric velocities from our model (solid lines) with the hydrodynamical simulations (dashed lines) of Kasen & Bildsten (2010). In this figure the opacities are set as $\kappa = 0.2\,\mathrm{cm^2\,g^{-1}}$, and $\kappa_\gamma = \infty$, in accord with Kasen & Bildsten (2010).

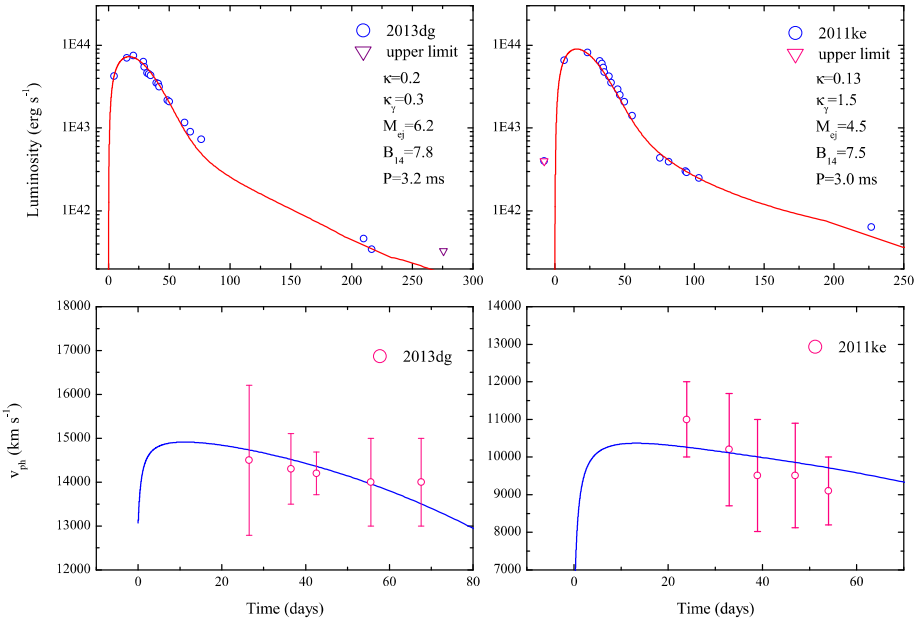

FIG. 9.— A demonstration of our analytical model to account for the flat velocity data points observed in most of the SLSNe. The light curve data for SNe 2011ke and 2013dg are taken from Inserra et al. (2013) and Nicholl et al. (2014), respectively. The velocity data points are taken from Nicholl et al. (2015).

simulations. This is the result of the diffusion approximation inherent in the analytical solution. As shown in this figure, increasing the dipole magnetic field (and thence reducing the spin-down time of the magnetar) of the magnetar results in a light curve of dimmer and short-lived. This again reinforces our conclusion that a magnetar with short spin-down timescale converts its rotational energy mostly into the kinetic energy of the SN, while the one with long spin-down timescale converts its rotational energy into the radiation of the SN. An SLSN is powered by a fast rotating (relatively) weakly magnetized magnetar. This stimulates us to speculate that the hypernovae, i.e. those SNe with kinetic energy $E_K > 10^{52}$ erg, could be powered by millisecond magnetars with much stronger dipole magnetic field.

The analytical model presented in this paper predicts a slow transition to nebular phase and a flat velocity curve. This is in immediate accord with the well known observational fact that SLSNe are usually slowly evolved compared to the normal type Ic SNe (e.g. Nicholl et al. 2015). As a demonstration, Figure 9 shows the light curves (the observational data are taken from Inserra et al. 2013 and Nicholl et al. 2014) and velocity curves of SLSNe 2013dg and 2011ke.[5] It can be seen that the model curves are in good agreement with the observational data. The flatness of the velocity curves of SLSNe is the result of two factors. First of all, SLSNe tend to be more massive than normal type Ic SNe (e.g. Nicholl et al. 2015). The magnetar, however, is another factor to make the velocity curve flat because the magnetar keeps accelerate the ejecta.

If it were not the effect of the magnetar, the photospheric velocity would keep declining because of the recession of the photosphere. The acceleration of the ejecta by magnetar partially compensates the photospheric recession. This fact may serve as a very interesting evidence in favor of the magnetar model against other alternative models. It can be tentatively concluded that the slow evolution to the nebular phase and the flat velocity curve of SLSNe are the result of the large ejecta mass and the existence of magnetar inherent to SLSNe. This gives justification for making more detailed modelling of the magnetar-powered SLSNe.

In this model the photospheric velocity first increases rapidly and then declines slowly. The inset of Figure 3, however, shows that the photospheric velocity of SN2010gx declines more rapidly than our model. This could be remedied by introducing an envelope as done by Inserra et al. (2013).

One issue we have deferred to discuss is the form of the energy flux from the magnetar. In its simplest form we just assume that the rotational energy of the magnetar is absorbed by the ejecta in the form of pure photons. Observation of pulsar wind nebulae (PWNe; Gaensler & Slane 2006; Hester 2008), however, indicates that the PWNe are usually a mixture of electron/positron pairs and magnetic (Poynting) flux. If the ejecta are massive enough, the rotational energy of the magnetar will eventually be completely absorbed, regardless of the existence of electron pairs or Poynting flux. If, however, the ejecta is less massive, e.g. $M_{\rm ej} = 10^{-4} - 10^{-2} M_\odot$, in the extreme case that the energy flux from the magnetar is completely lepton dominated, the outflow ejected by the double neutron star merger could be rapidly accelerated to relativistic speed and a strong reverse shock develops within the ejecta (Wang & Dai 2013; Wang et al. 2015a).

In most cases the PWNe behave neither in the Poynting-flux extreme, nor in the lepton-flux extreme, but rather lie in between. We therefore expect that the optical transients with mass as low as $M_{\rm ej} = 10^{-4} - 10^{-2} M_\odot$ would render their light curves as a trade-off of that studied in this paper and that given by Wang & Dai (2013) and Wang et al. (2015a, 2016), which we will study in the following papers.

We thank the referee for constructive suggestions that have allowed us to improve the manuscript. We also thank Yun-Wei Yu for helpful discussions. This work is supported by the National Basic Research Program ("973" Program) of China under Grant No. 2014CB845800 and the National Natural Science Foundation of China (grant Nos. U1331202, 11573014, and 11322328). D.X. acknowledges the support of the One-Hundred-Talent Program from the National Astronomical Observatories, Chinese Academy of Sciences. X.F.W. was also partially supported by the Youth Innovation Promotion Association (2011231), and the Strategic Priority Research Program "The Emergence of Cosmological Structure" (grant No. XDB09000000) of the Chinese Academy of Sciences.

APPENDIX

BASIC EQUATIONS AND THE NONHOMOLOGOUS SOURCE TERM

To help understand the link between Equations (46) and (11), we briefly list the equations governing the SN evolution as follows (Arnett 1980, 1982; Arnett & Fu 1989). The first law of thermodynamics is

$$\dot{E} + P\dot{V} = \epsilon - \frac{\partial L}{\partial m}, \tag{A1}$$

where E, V, ϵ are the thermal energy, volume, and heating rate of unit mass, respectively. $P(r,t)$, $L(r,t)$ are the pressure and luminosity at radius r, respectively. $m(r,t)$ is the ejecta mass within r. For a radiation gas, one has

[5] As for 2011ke, the first luminosity data point is coincident with an observational upper limit, as can be seen from Figure 12 in Inserra et al. (2013). After analyzing the data points, we think that the first data point is quite probably an upper limit because leaving this point as an upper limit results in a much better fit to the observational data. The data points presented here are therefore shifted by 7.9 days, both for the luminosity and velocity data points. As a result, of course, the fitting parameter values are different from those given by Inserra et al. (2013).

$E = aT^4V$ and $P = aT^4/3$. In the diffusion approximation

$$\frac{L}{4\pi r^2} = -\frac{\lambda c}{3}\frac{\partial aT^4}{\partial r} \tag{A2}$$

one finds that the energy conservation equation becomes

$$4T^4\left(\frac{\dot{T}}{T} + \frac{\dot{V}}{3V}\right) = \tilde{\epsilon} + \frac{1}{r^2}\frac{\partial}{\partial r}\left(\frac{c}{3\kappa\rho}r^2\frac{\partial T^4}{\partial r}\right), \tag{A3}$$

where

$$\tilde{\epsilon} = \frac{\epsilon}{aV}. \tag{A4}$$

In the adiabatic approximation, one has $T \propto R(t)^{-1}$. In order to determine the temperature distribution within the ejecta, we try to separate the dependence on space (r) and time (t)

$$T(r,t)^4 = \psi(x)\,\phi(t)\,T(0,0)^4\,R(0)^4/R(t)^4, \tag{A5}$$

where the dimensionless Lagrangian coordinate is defined as

$$x = r/R(t). \tag{A6}$$

With such a variable separation, the energy conservation equation becomes

$$\dot{\phi} + \frac{R}{R_0}\frac{\phi}{\tau_0} = \frac{b}{aT_0^4V_0}\frac{R}{R_0}f(t), \tag{A7}$$

where we have isolated an (assumed) constant

$$b \equiv \frac{\xi(x)\,\eta(x)}{\psi(x)} \tag{A8}$$

by assuming that the energy heating rate $\epsilon(r,t)$ can be separated in space and time

$$\epsilon = \xi(x)\,f(t) \tag{A9}$$

with $\xi(x)$ a dimensionless function. With these developments, it is easy to show that the SN luminosity is given by Equation (11). We therefore conclude that to include the nonhomologous expansion effect, one just needs to add S into the source term $\tilde{\epsilon}$. One caveat, however, is that by approximating b a constant, we actually assume that the heating rate distribution $\xi(x)$ is proportional to the temperature distribution $\psi(x)$, which is usually a good approximation. The nonhomologous source term S is far from such a distribution though. At the least, S is not positive definite. Consequently the nonhomologous effect cannot be accurately described by the simple prescription (11).

REFERENCES

Arnett, W. D. 1979, ApJL, 230, L37
Arnett, W. D. 1980, ApJ, 237, 541
Arnett, W. D. 1982, ApJ, 253, 785
Arnett, W. D., Fu, A. 1989, ApJ, 340, 396
Baltay, C., Rabinowitz, D., Hadjiyska, E., et al. 2013, PASP, 125, 683
Barnes, J. & Kasen, D. 2013, ApJ, 775, 18
Berger, E. 2007, ApJ, 670, 1254
Berger, E., Price, P. A., Cenko, S. B., et al. 2005, Natur, 438, 988
Canal, R., & Schatzman, E. 1976, A&A, 46, 229
Caraveo, P. A. 2014, ARA&A, 52, 211
Chatzopoulos, E., Wheeler, J. C., & Vinko, J. 2012, ApJ, 746, 121
Chatzopoulos, E., Wheeler, J. C., Vinko, J., et al. 2013, ApJ, 773, 76
Chomiuk, L., Chornock, R., Soderberg, A. M., et al. 2011, ApJ, 743, 114
Colgate, S. A., & McKee, C. 1969, ApJ, 157, 623
Colgate, S. A., Petschek, A. G., & Kriese, J. T. 1980, ApJL, 237, L81
Dai, Z. G., & Lu, T. 1998a, PhRvL, 81, 4301
Dai, Z. G., & Lu, T. 1998b, A&A, 333, L87
Dai, Z. G., Wang, S. Q., Wang, J. S., Wang, L. J., Yu, Y. W. 2016, ApJ, 817, 132
Dai, Z. G., Wang, X. Y., Wu, X. F., & Zhang, B. 2006, Science, 311, 1127
Dessart, L., Burrows, A., Ott, C. D., et al. 2006, ApJ, 644, 1063
Drake, A. J., Djorgovski, S. G., Mahabal, A., et al. 2009, ApJ, 696, 870
Ergma, E. V., & Tutukov, A. V. 1976, AcA, 26, 69
Gaensler, B. M., & Slane, P. O. 2006, ARA&A, 44, 17
Gal-Yam, A. 2012, Science, 337, 927
Giacomazzo, B., & Perna, R. 2013, ApJL, 771, L26
Grossman, D., Korobkin, O., Rosswog, S., & Piran, T. 2014, MNRAS, 439, 757
Hester, J. J. 2008, ARA&A, 46, 127
Hotokezaka, K., Kiuchi, K., Kyutoku, K., Okawa, H., & Sekiguchi Y. et al. 2013, PhRvD, 87, 024001
Huang, Y. F., Dai, Z. G., & Lu, T. 1999, MNRAS, 309, 513
Inserra, C., Smartt, S. J., Jerkstrand, A., et al. 2013, ApJ, 770, 128
Law, N. M., Kulkarni, S. R., Dekany, R. G., et al. 2009, PASP, 121, 1395
Levan, A. J., Wynn, G. A., Chapman, R., et al. 2006b, MNRAS, 368, L1
Kasen, D., Badnell, N. R., & Barnes, J. 2013, ApJ, 774, 25
Kasen, D., & Bildsten, L. 2010, ApJ, 717, 245
Korobkin, O., Rosswog, S., Arcones, A., & Winteler, C. 2012, MNRAS, 426, 1940
McCrum, M., Smartt, S. J., Kotak, R., et al. 2014, MNRAS, 437, 656
Metzger, B. D. 2012, MNRAS, 419, 827
Metzger, B. D., Arcones, A., Quataert, E., Martinez-Pinedo, G. 2010a, MNRAS, 402, 2771
Metzger, B. D., Margalit, B., Kasen, D., Quataert, E. 2015, MNRAS, 454, 3311
Mösta, P., Ott, C. D., Radice, D., et al. 2015, Natur, 528, 376
Nicholl, M., Smartt, S. J., Jerkstrand, A., et al. 2014, MNRAS, 444, 2096
Nicholl, M., Smartt, S. J., Jerkstrand, A., et al. 2015, MNRAS, 452, 3869
Nomoto, K., & Kondo, Y. 1991, ApJL, 367, L19
Ostriker, J. P., & Gunn, J. E. 1971, ApJL, 164, L95
Papadopoulos, A., D'Andrea, C. B., Sullivan, M., et al. 2015, MNRAS, 449, 1215
Quimby, R. M., Kulkarni, S. R., Kasliwal, M. M., et al. 2011, Nature, 474, 487
Rau, A., Kulkarni, S. R., Law, N. M., et al. 2009, PASP, 121, 1334
Rezzolla, L., Baiotti, L., Giacomazzo, B., et al. 2010, CQGra, 27, 114105
Roberts, L. F., Kasen, D., Lee, W. H., & Ramirez-Ruiz, E. 2011, ApJL, 736, L21
Rosswog, S., Piran, T., & Nakar, E. 2013, MNRAS, 430, 2585
Saio, H., & Nomoto, K. 1985, A&A, 150, L21
Soderberg, A. M., Berger, E., Kasliwal, M., et al. 2006, ApJ, 650, 261
Tanaka, M., & Hotokezaka, K. 2013, ApJ, 775, 113
Usov, V. V. 1992, Nature, 357, 472
Wang, L. J., & Dai, Z. G. 2013, ApJL, 774, L33
Wang, L. J., Dai, Z. G., & Yu, Y. W. 2015a, ApJ, 800, 79
Wang, L. J., Dai, Z. G., Liu, L. D., & Wu, X. F. 2016, ApJ, in press, (arXiv:1603.08208)
Wang, S. Q., Liu, L. D., Dai, Z. G., Wang, L. J., & Wu, X. F. 2015b, arXiv:1509.05543
Wang, S. Q., Wang, L. J., Dai, Z. G., & Wu, X. F. 2015c, ApJ, 799, 107
Wang, S. Q., Wang, L. J., Dai, Z. G., & Wu, X. F. 2015d, ApJ, 807, 147
Woosley, S. E. 2010, ApJL, 719, L204
Yu, Y. W., Zhang, B., & Gao, H. 2013, ApJL, 776, L40
Zhang, B. 2013, ApJL, 763, L22